Applications of SSM/I Data in the Analysis of Hurricane Florence (1988)

RANDALL J. ALLISS

Department of Marine, Earth and Atmospheric Sciences, North Carolina State University, Raleigh, North Carolina

GLENN D. SANDLIN AND SIMON W. CHANG

Naval Research Laboratory, Washington, D.C.

SETHU RAMAN

Department of Marine, Earth and Atmospheric Sciences, North Carolina State University, Raleigh, North Carolina

(Manuscript received 10 June 1992, in final form 23 March 1993)

ABSTRACT

Data from the Special Sensor Microwave/Imager (SSM/I) on board a Defense Meteorological Satellite Program satellite are used to study the precipitation patterns and wind fields associated with Hurricane Florence (1988). SSM/I estimates indicate that the intensification of Florence was coincident with the increase in total latent heat release. Additionally, an increase in the concentration and areal coverage of heavier rain rates near the center is observed. SSM/I marine surface winds of Florence are examined and compared to in situ data, and to an enhanced objective isotach analysis over the Gulf of Mexico. Results indicate that the SSM/I winds are weaker than those depicted in the enhanced objective analysis and slightly stronger than in situ observations. Finally, center positions of Florence are estimated using the 85-GHz brightness-temperature imagery. Much improved estimates are achieved using this imagery compared to using GOES infrared imagery. These results concur with previous studies that applications of SSM/I data could be valuable in augmenting current methods of tropical cyclone analysis.

1. Introduction

The advent of the meteorological satellite in the 1960s has significantly improved tropical cyclone detection, analysis, and prediction. The geostationary satellites provide imagery (e.g., every half-hour) in the visible (VS), infrared (IR), and water vapor channels on a routine basis. Sensors flown aboard polar-orbiting satellites, like the Advanced Very High Resolution Radiometer (AVHRR), which has higher IR resolution than the geostationary satellites, have been beneficial to the forecaster in observing tropical cyclones. In June of 1987, the first Special Sensor Microwave/Imager (SSM/I) was launched aboard a Defense Meteorological Satellite Program (DMSP) satellite. The polar-orbiting SSM/I provides data in seven microwave channels for both land and atmospheric remote sensing.

SSM/I algorithms that relate polarized microwave brightness temperatures (BT) to certain atmospheric parameters, including rain rates and wind speeds, can be used to study tropical cyclones (Rodgers and Adler 1981). Emitted microwave radiation at 85.5 GHz can penetrate the overlying cirrus clouds, commonly associated with hurricanes, with limited attenuation, revealing the low-level center, which can be inferred from the convective organization. With a resolution of approximately 12.5 km, the center position of developed tropical cyclones without visible eyes can be better estimated using 85-GHz imagery than by using conventional visible and infrared imagery alone (Velden et al. 1989).

The objective of this article is to present SSM/I rainfall rates and other precipitation parameters during various stages of Atlantic Hurricane Florence's (1988) development. Comparisons are made between the precipitation patterns of Florence and those of devastating Hurricane Hugo (1989). During Florence's short life, it went through episodes of rapidly changing convective activity (Rodgers et al. 1991). Because Florence only reached minimal hurricane strength, its intensity may have been greatly modulated by the convection. Florence was captured in SSM/I imagery every 12 h during a 3-day period. In addition to the SSM/I precipitation rates, SSM/I near-surface wind speeds were retrieved to determine the extent of near tropical storm–force winds (≥ 15 m s^{-1}). These SSM/I wind speeds are compared to in situ data and to an enhanced objective isotach analysis that includes dropsonde data (Shi et

Corresponding author address: Dr. Simon W. Chang, Naval Research Laboratory, Code 7225, Department of the Navy, Washington, DC 20375-5000.

al. 1991). Finally, SSM/I estimates of storm location are compared to the National Hurricane Center (NHC) best-track data.

2. Special Sensor Microwave/Imager (SSM/I)

The SSM/I is a passive radiometric system that measures the upwelling radiation from the surface of the earth and atmosphere. The SSM/I is aboard a DMSP polar-orbiting satellite that orbits the earth in a near sun-synchronous mode at an altitude of 833 km, and with an orbital period of 102 min. The SSM/I completes 32 scans per minute over a swath of 1400 km, and measures upwelling radiation at 19.3, 22.2, 37.0, and 85.5 GHz. By initial design, all but the 22-GHz channel provide BT for the vertical (V) and horizontal polarizations (H). The 22-GHz channel measures only V polarized radiation. Each channel has a different-sized footprint. See Hollinger et al. (1991) for more detailed information on the graphic description of the footprint geometry. The 85-GHz channel has the smallest footprint (15 km × 13 km) while the 19-GHz channel has the largest (69 km × 43 km). The imager senses an average emission from each footprint. Although the footprint sizes of each channel are different, a 25-km resolution is representative of the combined channels used in the algorithms and is thus selected for the resolution of the precipitation and wind data.

a. *Rainfall-rate algorithm*

The rain-rate algorithm used in this study is described by Olson (1989) and Hollinger (1991). Since the 85-GHz V channel was unavailable during September 1988, an alternative algorithm is applied using the 85-GHz H channel, as well as the 22-GHz V, 37-GHz V and H channels, and the 19-GHz V and H channels. Pixels within ±100 km of the coast were not processed because of possible ambiguity, although additional algorithms for the land–sea interface are now being developed (Adler 1992, personal communication). The recommended alternate algorithm (Hollinger 1991) is used.

Over ocean:

$$R = \exp(-0.42383 - 0.0082985T_{85h} + 0.01496T_{19v} + 0.00583T_{19h}) - 4.0 \text{ mm h}^{-1}, \quad \text{and} \quad (1)$$

over land:

$$R = \exp(1.32526 - 0.08150T_{37v} + 0.01638T_{37h} + 0.03561T_{22v} + 0.05079T_{19v} - 0.01875T_{19h}) - 8.0 \text{ mm h}^{-1}, \quad (2)$$

where R is the rainfall rate and T_{37v}, T_{37h}, T_{19v}, T_{19h}, T_{22v}, and T_{85h} are the BTs of the 37-GHz V, 37-GHz H, 19-GHz V, 19-GHz H, 22-GHz V, and 85-GHz H channels, respectively. If the formulas produced a rainfall rate less than zero, then the rain rate value was set equal to zero.

SSM/I-derived rainfall rates using this algorithm have been statistically validated by comparisons with radar estimates (Olson 1989). The rainfall-rate validation was conducted by obtaining ground truth from radars at both the Marshall Islands, Kwajalein, and Darwin, Australia. Additionally, seven radars in the United Kingdom and one located at Cape Canaveral, Florida, were used in the validation. SSM/I rainfall rates were found to have a standard deviation of 5 mm h^{-1} over the rainfall rate range of 0–25 mm h^{-1}.

b. *Wind speed algorithm*

The SSM/I wind speed algorithm was designed to retrieve wind speeds over the oceans and to be valid at 19.5 m above the ocean surface. The magnitude of microwave energy being emitted from the ocean surface is dependent on the wave structure and foam coverage, which in turn are influenced by the wind speed. Therefore, by measuring the ocean surface microwave emission, the SSM/I is able to infer the ocean surface wind speed. The 19-GHz V and 37-GHz H polarized channels are most sensitive to the ocean roughness and foam (Goodberlet et al. 1989). The wind algorithm utilizes two other channels: the 22-GHz V and 37-GHz V channels, to account for atmospheric attenuation effects. The 22-GHz V channel is used to address atmospheric water vapor effects, while the difference between the 37-GHz V and 37-GHz H channels (37V − 37H) is used to detect cloud and liquid water scattering (Goodberlet et al. 1989). The algorithm for wind speed (WS) used in this study (Hollinger 1991) is:

$$\text{WS} = 147.90 + 1.0969T_{19v} - 0.4555T_{22v} - 1.7600T_{37v} + 0.7860T_{37h}, \quad (3)$$

where T_{22v} is the BT of the 22-GHz V polarized channel and the other variables are as given previously.

Currently, there are two fundamental limitations to the accuracy of SSM/I wind speed retrievals: the resolution of the instrument and the presence of cloud water, rain, and hail in the atmosphere. Upwelling microwave energy at the SSM/I frequencies, which is coming from the ocean surface, can be masked by the emission and attenuation characteristics of rain and hail in the earth's atmosphere. Therefore, "rain flags" have been established to estimate the degree of uncertainty of each calculated wind speed due to the presence of intervening water vapor, cloud water, rain, or hail (Goodberlet et al. 1989). The SSM/I wind speed uncertainties for the respective rain flags are listed in Table 1. Additionally, the effective resolution of the algorithm is limited by the resolving power of the SSM/I antenna at 19, 22, and 37 GHz, which can act to smooth the high spatial gradients in wind speed present in nature.

SSM/I wind speeds have been validated by comparisons with NOAA buoys, and found to have an ac-

TABLE 1. SSM/I rain flags and their standard deviations (after Goodberlet et al. 1989).

Rain flag	Standard deviations of wind speed (m s^{-1})
0	<2
1	2–5
2 and 3	>5

curacy of ±2 m s^{-1} between 3 and 25 m s^{-1}, within which 85% of the retrievals occurred. For the remaining 15% of the retrievals, winds are flagged, and are progressively uncertain with increasing flag numbers as atmospheric attenuation increases (Goodberlet et al. 1989). Wind speeds above 25 m s^{-1} have not been validated.

3. Hurricane Florence

The circulation that eventually became Hurricane Florence developed within an area of disturbed weather located in the south-central Gulf of Mexico on 7 September 1988. This area of convection had previously been associated with a cold front that had entered the Gulf of Mexico from the north several days earlier. This system subsequently strengthened and became Tropical Storm Florence. According to NHC best-track data, Florence tracked eastward and then northward on 8 September. On 9 September, Florence began to accelerate toward the north and intensify. By 1800 UTC 9 September, Florence had become a hurricane just south of New Orleans. An air force reconnaissance aircraft reported maximum sustained winds of 33 m s^{-1} at this time and estimated a minimum central pressure of 985 mb. Florence made landfall in southeastern Louisiana at 0200 UTC 10 September. After landfall, Florence rapidly weakened as it moved northwest and dissipated over eastern Texas on 11 September (Lawrence and Gross 1989). Figure 1 shows the track of Florence.

4. SSM/I precipitation patterns of Florence

Six SSM/I images of Florence were obtained at approximately 12-h intervals from tropical depression stage through final landfall. Rainfall rates from each pass beginning 1200 UTC 7 September through 0000 UTC 10 September were compiled and interpolated onto a grid with a horizontal resolution of 0.25° in longitude and latitude. Figure 2a reveals the SSM/I precipitation rates at 1200 UTC 7 September. At this time, Florence was classified as a tropical depression by NHC. Maximum sustained winds were estimated to be 15 m s^{-1}. The rain-rate imagery shows a small pocket of rain rates greater than 20 mm h^{-1} embedded within a larger area of lighter rainfall just to the northwest of the Yucatan Peninsula. The area of relatively heavier precipitation of greater than 20 mm h^{-1} at this time is placed to the south of the center.

Twelve hours later at 0000 UTC 8 September, SSM/I rain-rate imagery reveals that the precipitation field has expanded with a larger area of rain rates greater than 20 mm h^{-1} (Fig. 2b). Additionally, a cyclonic curvature is now evident in the overall precipitation pattern. Florence was upgraded to a tropical storm by NHC at this time when maximum sustained winds were estimated to be 23 m s^{-1}. The SSM/I image at this time showed a weak north–south-oriented rainband present to the north of the main area of convection. The low-level center, as indicated by the best-track data during this time, was still to the north of the deep convective region.

The pass at 1200 UTC 8 September reveals two areas of heavy precipitation (Fig. 2c). The first, along the northwest coast of the Yucatan Peninsula, is associated with Florence. The second area is located over the northeastern Gulf of Mexico and is associated with a stalled frontal system that extends from the northeast Gulf of Mexico to the southeast coast of the United States. The area of precipitation associated with Tropical Storm Florence with rain rates greater than 20 mm h^{-1} have grown considerably during this time.

The two SSM/I images of Florence on 9 September capture the rapid intensification of the precipitation patterns on this day. The areal coverage of intense precipitation at 0000 UTC (Fig. 2d) associated with Florence is considerably less than the previous SSM/I pass. The intensity decreased slightly over this 12-h period with a 2-mb central pressure increase. Over the next 12 h, however, two areas of convection developed

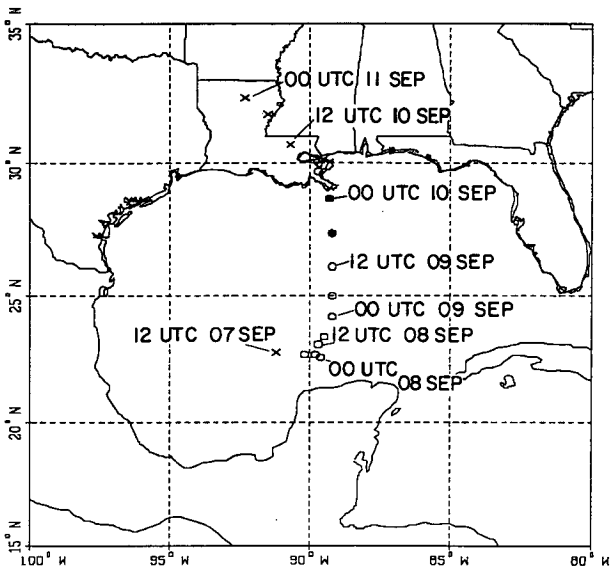

FIG. 1. Track of Hurricane Florence every 6 h from depression stage through final landfall: X—tropical depression stage, O—tropical storm stage, and ●—hurricane stage. Times and dates are indicated at 0000 and 1200 UTC each day.

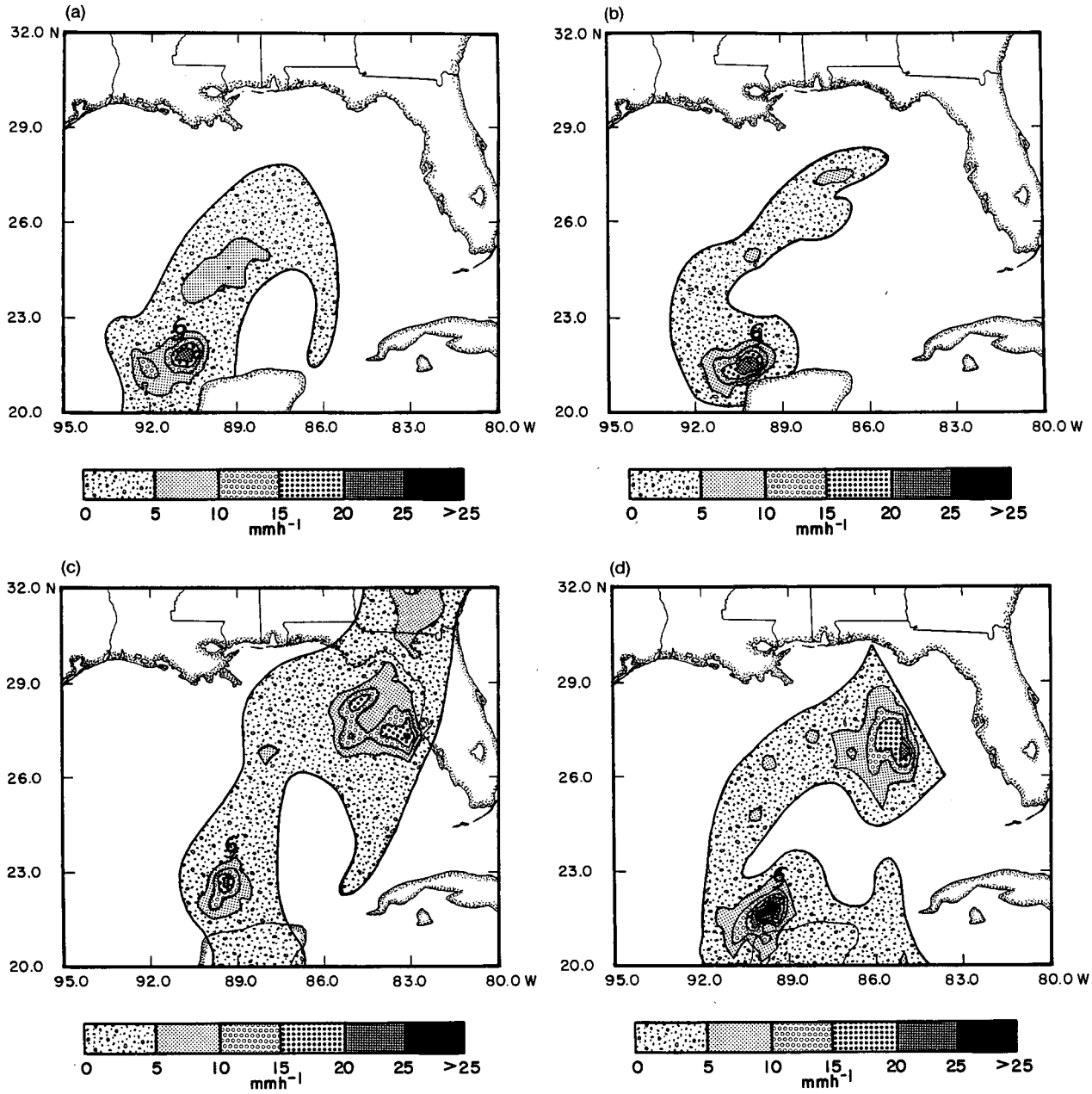

FIG. 2. (a) SSM/I rainfall rates at 1200 UTC 7 September 1988. The legend for all rain rate displays is indicated on the figure; (b) same as (a) except for 0000 UTC 8 September 1988; (c) same as (a) except for 1200 UTC 8 September; (c) same as (a) except for 0000 UTC 9 September; (e) same as (a) except for 1200 UTC 9 September; and (f) same as (a) except for 0000 UTC 10 September. The tropical storm symbol on each figure indicates the center of Florence during that pass.

around the center of Florence (Fig. 2e). The SSM/I image at 1200 UTC 9 September shows the explosive increase in the areal coverage of Florence's precipitation pattern. Rain rates greater than 25 mm h^{-1} are present to the northwest and southeast of the low-level center. These areas of heavy precipitation, as expected, are exactly coincident with the deeply convective regions seen in the GOES infrared imagery at 1200 UTC (Fig. 4 of Rodgers et al. 1991). The low-level center of Florence at this time is marked by a minimum in SSM/I rainfall rates. A large rainband is also observed in the precipitation field emanating from the northernmost convective region and extending south along the east coast of the Yucatan.

Figure 3 reveals a west-to-east cross section of rainfall rates through the center of Florence at 1200 UTC 9 September. The presence of two maxima in rainfall on either side of the center is evident. Rainfall rates of 19

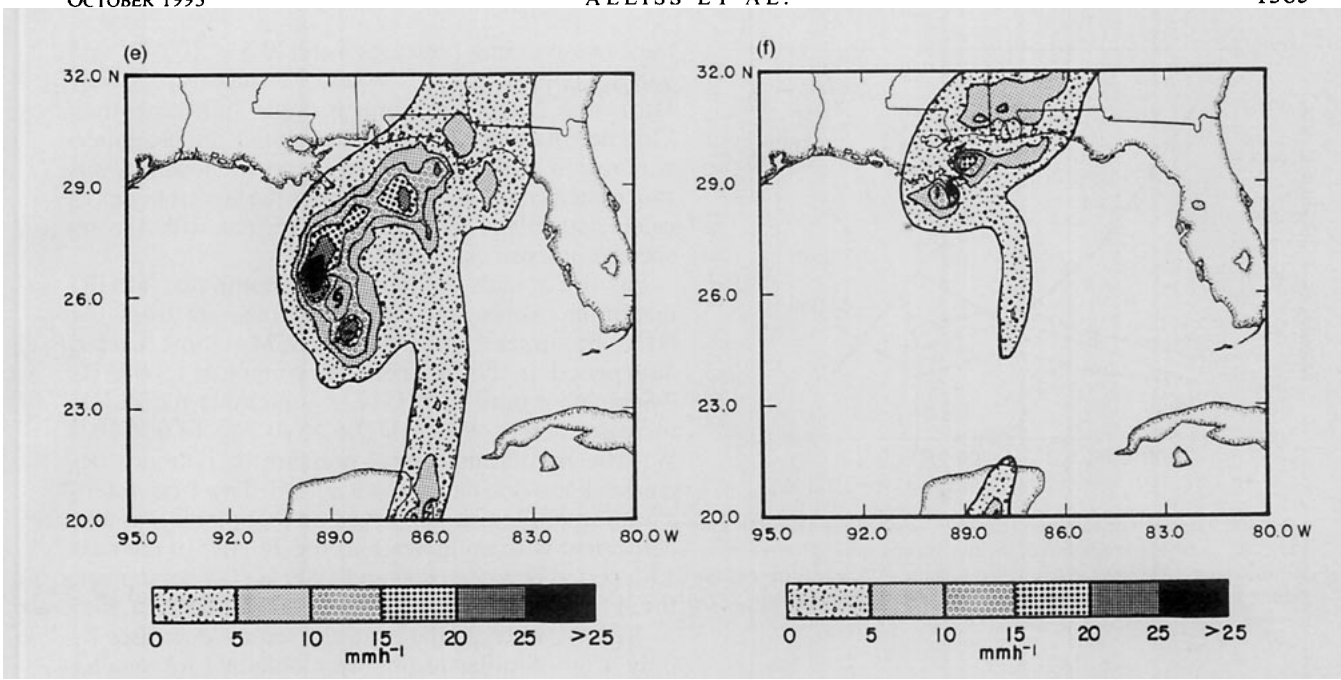

FIG. 2. (*Continued*)

and 12 mm h^{-1} are evident on the west and east sides of the center, respectively, with a minimum of 2.5 mm h^{-1} in the center. A small secondary maximum is also noted 330 km to the east of the center, associated with the rainband shown in Fig. 2e.

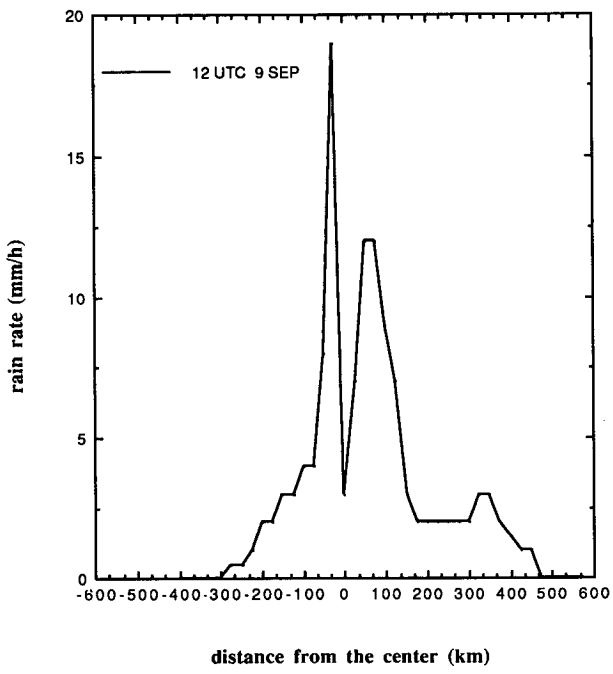

FIG. 3. West-to-east cross section of rain rates through the center of Florence at 1200 UTC 9 September. Refer to Fig. 2f for the location of the cross section. Maximum rainfall rates of 19 and 11 mm h^{-1} are evident on the west and east sides of the eyewall, respectively. A minimum value of 2.5 mm h^{-1} is observed in the eye region.

Several hours prior to the SSM/I overpass at 0000 UTC 10 September, Florence had reached its maximum intensity. The center of circulation determined by NHC was located just south of the Mississippi delta. SSM/I 85-GHz imagery revealed an intrusion of dry air into the circulation from the west and southwest (not shown). As a result, the convection had become weak and disorganized. SSM/I rain rates at 0000 UTC confirm this weakening (Fig. 2f). Although precipitation is evident, all heavy precipitation has diminished with no rain rates greater than 10 mm h^{-1} found near the center. The decrease in rain rates at this time is in agreement with the radar reflectivities of the NWS WSR-57 at Slidell, Mississippi (Hollinger 1989).

5. Other rainfall characteristics

a. SSM/I-derived parameters

The average rain rates within radii of 111, 222, and 444 km of the center are computed and evaluated for each SSM/I pass. Figure 4 shows the 111-km average rain rate (mm h^{-1}) versus the minimum central pressure as a function of time. Calculations are made over a 2-day period during which Florence strengthened from a tropical depression to a strong tropical storm. The SSM/I data just prior to landfall were excluded from the calculation due to the land contamination. Figure 4 reveals that the average rain rate within the 111-km radius is highly correlated with the central sea level pressure. The increase in rainfall is especially notable between the 0000 UTC 9 September and 1200 UTC 9 September passes in which the average rain rate increases from 3.0 to more than 13 mm h^{-1}. During the same period, the minimum central pressure drops

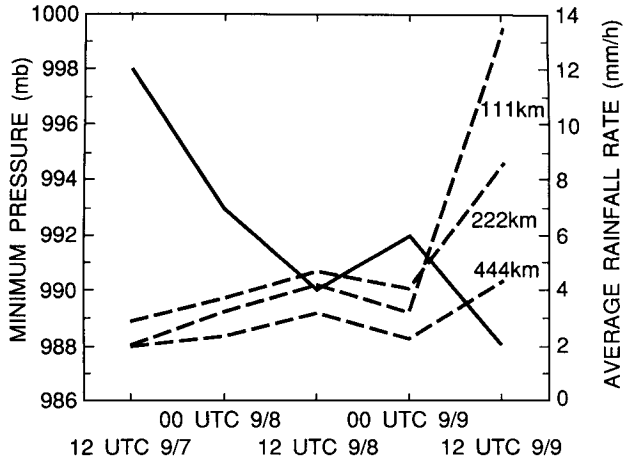

FIG. 4. The average rain rate (mm h^{-1}, dashed lines) within an 111-, 222-, and 444-km radius of the center versus minimum central pressure (mb, solid line) as a function of time. A decrease in central pressure corresponds to an increase in the average rain rate.

from 992 to 988 mb. The average rain rates within the 222- and 444-km radii also show the same correlation with Florence's intensity. The average rain rate within the 222-km radius is larger than that of the 111 km between 1200 UTC 7 September and 0000 UTC 9 September, indicating that the heavier precipitation is located off the storm center. A standard Student's t-test is conducted to determine the correlation between the average rain rate (111-km radius) and minimum pressure. A correlation coefficient of −0.93 was found significant at the 2% level. This suggests that there is a strong association between the increase or decrease in SSM/I rain rates and the intensity of Florence. Similar results were obtained for Hurricane Hugo of 1989 (Alliss et al. 1992).

The total latent heat release (TLHR) for five SSM/I observations is evaluated for a circular area with a radius of 444 km from the center. The center for all passes was determined by an analysis of the 85-GHz imagery. The TLHR over an area is given by

$$\text{TLHR} = L\rho \int_A R da, \qquad (4)$$

where ρ is the density of rainwater assumed to be 1.0×10^3 kg m^{-3}, L, the latent heat of condensation (2.5×10^6 J kg^{-1}), da, the incremental area (27 km^2), R, the rainfall rate at each grid point, and A, the area of integration.

The time-averaged TLHR within 444 km of the center of Florence is calculated to be 11.5×10^{14} W. This estimate results from five passes over a 48-h period during which time Florence's intensity was mostly below hurricane strength. By comparison, Alliss et al. (1992) found for eight SSM/I observations of Hurricane Hugo of 1989 an average TLHR of 16.6×10^{14} W. At Hugo and Florence's peak intensities the maximum TLHR within 444 km radius of the center and the corresponding pressures were 20.5×10^{14} W and 918 mb and 17.5×10^{14} W and 988 mb, respectively. Hurricane Hugo was a much larger hurricane than Florence, having a well-developed and intense inner-core region. The inner core of Florence, however, was much smaller and less defined, thus the large differences calculated in the TLHR are consistent with the respective intensities.

Figure 5 reveals the trend of the computed TLHR, maximum winds, and minimum pressure from the NHC best-track data for each SSM/I time over a 48-h period. In the 24-h period beginning at 1200 UTC 7 September until 1200 UTC 8 September the TLHR increases nearly 60% from 7.6×10^{14} to 13.0×10^{14} W. The minimum central pressure of Florence decreases 8 mb during this 24-h period. The 4-mb intensification of Florence observed on 9 September is also coincident with an increase in the TLHR. In the next 12-h period between 0000 and 1200 UTC 9 September, the TLHR increases 55% from 9.5×10^{14} to 17.5×10^{14} W, whereas the central pressure decreases by only 4 mb. Similar results were obtained for smaller radii calculations of TLHR. Unfortunately, Florence starts to be influenced by land shortly after 1200 UTC 9 September, a long persistent trend, and the lag between precipitation and intensity in a relatively uniform environment cannot be observed.

b. *Spatial variations of rainfall rates*

The contributions of rainfall within specified rain-rate categories and the areal coverage of these rain rates were examined during Florence's intensification episode on 9 September. Figures 6a and 6b show the percent areal coverage of rainfall and the percent contribution of rainfall for four rain-rate categories within 200 km of the center. Figure 6a reveals the distribution

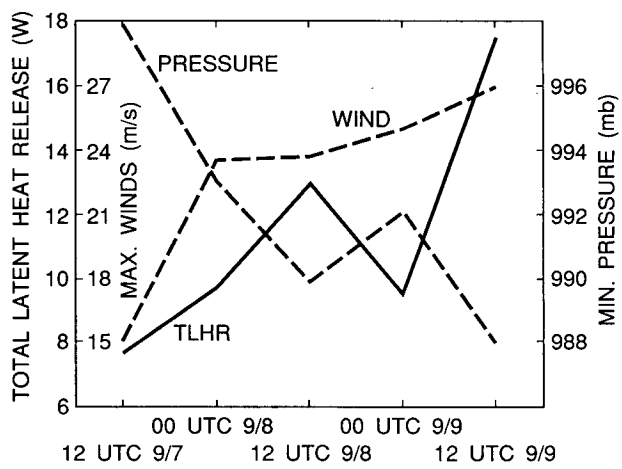

FIG. 5. Total latent heat release ($\times 10^{14}$ W) within a 444-km radius of the center as a function of time for Florence. Minimum pressure (mb) and maximum winds (m s^{-1}) are also shown for each SSM/I pass. All wind and pressure data was obtained from the NHC best-track data.

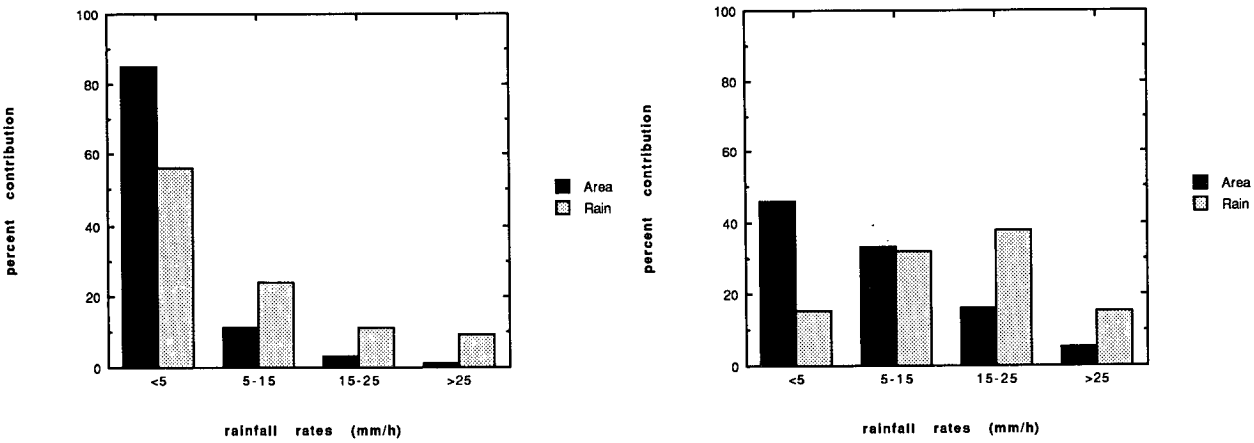

FIG. 6. Percent areal coverage (black shade) and percent contribution (dotted shade) of rainfall by four rain-rate categories within a radius of 200 km from the center for (a) 0000 UTC 9 September and (b) 1200 UTC 9 September.

at 0000 UTC 9 September when a minimum pressure of 992 mb was estimated. Rain rates less than 5 mm h^{-1} occur in 85% of the area and contribute to 56% of the total precipitation. Rates greater than 15 mm h^{-1} occur in only 4% of the area and contribute to only 20% of the total rainfall. Due to the absence of deep convection, high rain rates were not the dominant feature in Florence during this pass.

As the storm intensified over the next 12 h, the intensity and coverage of the rainfall also increased. A major shift in the rain-rate distribution is noted during the SSM/I observation at 12 UTC 9 September. Figure 6b indicates that rates less than 5 mm h^{-1} now occur in only 46% of the area and contribute to less than 15% of the total rainfall. Rates between 15 and 25 mm h^{-1} occur in 16% of the area and contribute to nearly 40% of the total rainfall. The increasingly important contribution of heavier rainfall becomes evident during this pass. Percentage areal coverage and percentage amount contribution (in brackets) of rates greater than 25 mm h^{-1} increase from 1% (9%) at 0000 UTC to 5% (15%) at 1200 UTC. It appears that as Florence intensified, both the areal and amount contribution of heavier precipitation within the 200-km radius increase. These observations concur with those results obtained for Hurricane Hugo (1989). The overall magnitude of the percent areal coverage and the percent contribution of rainfall greater than or equal to 15 mm h^{-1} in Florence is 40% of what is observed for the same category in Hugo. This difference is probably due to the large contrast in intensity.

The azimuthally averaged spatial distribution of rainfall as a function of distance from the center is computed for the two SSM/I overpasses on 9 September. Figure 7 shows the average rainfall rate for each 20-km radius from the center during the intensification episode. As Florence intensifies, the maximum average rain rate within each radius also increases. More importantly, the maximum rainfall moves closer to the center from 0000 to 1200 UTC, suggesting the development of inner-core convection. At 0000 UTC, the maximum average rain rate is 5 mm h^{-1} at 130 km from the center. Twelve hours later, a maximum value of 16 mm h^{-1} is reached 70 km from the center. During this period, the minimum sea level pressure of Florence decreases from 992 to 988 mb. In the case of Hugo (1988), it is also found that the maximum precipitation shifts toward the center as Hugo intensifies (Fig. 13 in Alliss et al. 1992). There, the maximum precipitation rates are between 15 and 20 mm h^{-1}, reflecting the much stronger intensity compared to Florence. Furthermore, the double eyewall observed in Hugo, which may have contributed to its intensity changes, is not apparent in Florence.

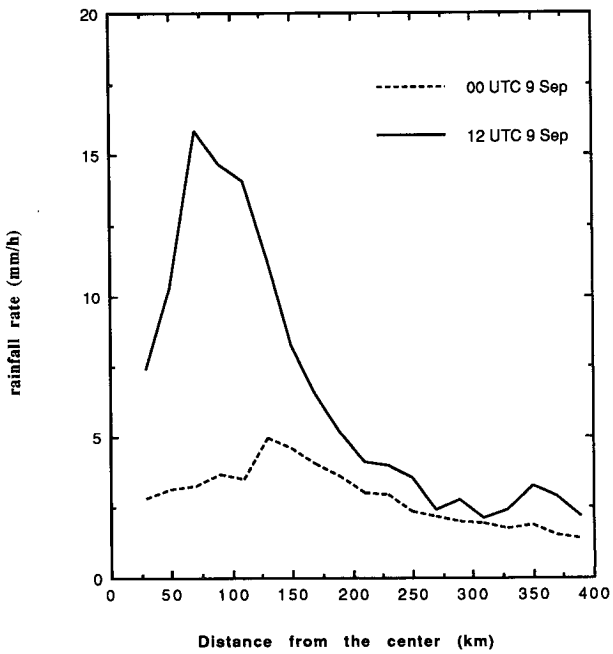

FIG. 7. Average rainfall rate as a function of distance from the storm center for 0000 and 1200 UTC 9 September.

6. SSM/I wind speed observations

Surface wind measurements over the open oceans are sparse and mainly limited to buoys and ships of opportunity. The majority of these reports originate in shipping lanes and along coastlines, most of which lie outside the tropics. These platforms do not provide a complete description of the horizontal distribution of surface wind speeds. Moreover, ships that do report winds avoid regions of stormy weather. In this section, we evaluate the usefulness of SSM/I-derived winds in the Florence case.

Fifty-one Omega dropwindsondes (ODWs) were deployed by the Atlantic Oceanographic and Meteorological Laboratories/Hurricane Research Division (AOML/HRD) during a synoptic flow experiment centered on Hurricane Florence on 8–9 September 1988. The data collected were employed to enhance a regional analysis and forecast system analysis of Florence's surface wind field at 0000 UTC 9 September (Shi et al. 1991). The enhanced analysis is used for comparison with SSM/I-derived wind speeds here. The ODW data used in the analysis were collected between 2100 UTC 8 September and 0300 UTC 9 September and assumed valid at 0000 UTC.

A second validation of SSM/I-derived wind speed observations is presented. In this case, a set of ship and buoy observations at 1200 UTC 9 September are compared with the SSM/I winds.

As discussed in section 2b, a set of rain flags is devised to indicate the reliability of the retrieval because the SSM/I marine surface wind retrieval is easily affected by atmospheric attenuations. In the following discussion, the retrieved wind speed will be presented along with the rain flags, indicating the quality of the retrieval.

a. SSM/I winds at 0000 UTC 9 September

Figure 8a shows SSM/I wind speeds (rain flag 0) rounded to the nearest meter per second at 0000 UTC 9 September. At this time, the center of Florence was near 24.2°N, 89.2°W. These wind speed estimates occur where the atmospheric attenuation is quite small, and thus represent the highest reliability. The majority of the rain flag 0 wind speed estimates within this swath are less than 15 m s^{-1} and occur outside the precipitation of Florence's inner region and the coastal front (see Fig. 2d). Furthermore, only 40% of the SSM/I wind retrievals during this pass in the Gulf of Mexico are of rain flag 0 quality.

In this SSM/I overpass, more than 30% of the SSM/I wind speeds are of rain flag 1 quality. Here a method is devised to include wind speed retrieval with flag 1 so that more retrieved winds can be used and displayed. The method uses the probability that a rain flag 1–derived wind speed yields an actual wind of at least 15 m s^{-1}. The 15 m s^{-1} threshold is chosen because it is close to the gale-force wind. We assume that there is a Gaussian distribution in the probability of actual wind speeds for a given retrieved wind speed. According to Table 1, the wind speeds with flag 1 quality have a standard deviation of no larger than 5 m s^{-1}. Therefore, for example, if the algorithm yields a 20 m s^{-1} wind speed it will have at least an 84% chance that the actual wind speed is at least 15 m s^{-1} and a 16% probability that the actual wind is less than 15 m s^{-1}. Table 2 shows the probability of tropical storm winds based on rain flag 1 wind speeds.

Figures 8a and 9 display the area with different probabilities of occurrence of wind speeds greater than or equal to 15 m s^{-1}. The few large asterisks in Fig. 8a denote where there is at least a 84% probability of wind speeds larger than 15 m s^{-1}. The small crosses in Fig. 8a indicate a range of 50%–84% likelihood of such occurrence and the very small dots indicate a less than 50% probability. Only a small area east of the center suggests the actual winds may be as high as 15 m s^{-1}. The majority of the area in the flag 1 region outside the precipitation is experiencing less than 15 m s^{-1} winds at 0000 UTC. The large dots in Fig. 8a indicate rain flags 2 and 3, where attenuation due to heavy precipitation results in unreliable SSM/I wind speeds (refer to Table 1).

Figure 8b shows the ODW-enhanced 1000-mb-level isotach analysis at 0000 UTC 9 September of Shi et al. (1991) superimposed on the SSM/I-derived wind speeds valid at the same time. The integers in Fig. 8b represent both rain flag 0 and 1 wind speeds. Throughout the entire region covered by Florence, the SSM/I wind speeds are, in general, underestimated compared to the enhanced analysis. The isotach analysis shows that winds greater than 15 m s^{-1} are present in areas to the east and west of Florence's center. Furthermore, large gradients in the wind field are present over the same region in the isotach analysis, which is not well resolved by the SSM/I. In the ODW data, winds below the 950-mb level are normally not reported. Therefore, winds below the lowest reporting levels in the enhanced analysis of Shi et al. are assumed to be the same as those at the lowest reporting levels. This may lead to an overestimate of the 1000-mb winds in the analysis.

b. SSM/I winds at 1200 UTC 9 September

The SSM/I wind estimates for 1200 UTC 9 September are shown in Fig. 9. At this time, the center of Florence was located at 26.1°N, 89.2°W. For rain flag 0 wind speeds, maximum winds obtained from the algorithm are no greater than 16 m s^{-1}. Since the precipitation shield associated with Florence has expanded by this time, the majority of the area is dominated by rain flags greater than zero. The high likelihood, however, that winds equal or exceed tropical storm force is apparent near the western and eastern periphery of the storm's inner-core region. As mentioned in the above, the presence of precipitation greatly affects the SSM/I wind reliability. This is evident in Fig. 9 as the spatial pattern of rain flags 2 and 3 are highly repre-

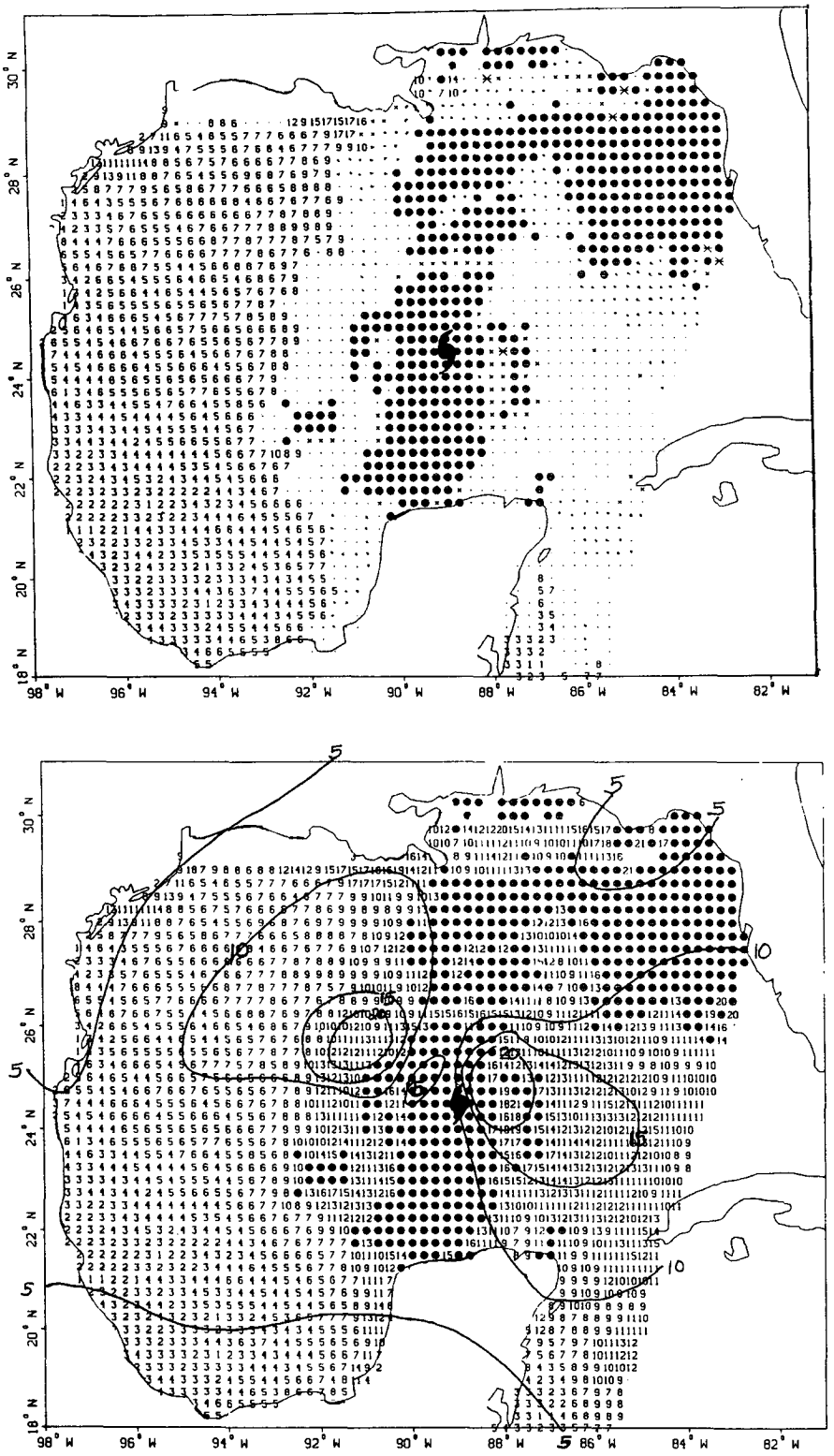

FIG. 8. (a) SSM/I-derived winds at 0000 UTC 9 September. All values indicate rain flag 0 wind speeds ($m\ s^{-1}$). Asterisks, crosses, and solid dots indicate the range of probabilities for winds of at least 15 $m\ s^{-1}$ as indicated in Table 2. Blank areas indicate missing data. Large dots indicate rain flag 2 and 3 wind speeds. The hurricane symbol denotes the location of the low pressure center. (b) Isotach analysis based on ODW observations with a 5 $m\ s^{-1}$ isotach interval superimposed on the SSM/I wind speed estimates at 0000 UTC 9 September. SSM/I wind speeds with flag 0 and 1 are in meters per second.

TABLE 2. The probability that an SSM/I-derived wind speed with a rain flag of 1 is at least 15 m s^{-1}. The method assumes a Gaussian distribution of the estimated wind speed.

Estimated rain flag 1 wind speed (m s^{-1})	Probability of 15 m s^{-1} wind
≥20	>84%
15–20	50%–84%
<15	<50%

sentative of the extensive precipitation field observed by SSM/I (Fig. 2e).

For comparison, reported buoy and coastal station winds in the Gulf of Mexico region at 1200 UTC are listed in Table 3. The latitude, longitude, and observed wind speed are shown, along with the nearest SSM/I wind speed and its corresponding rain flag. Three of the seven comparisons were for rain flag 0 wind speeds, all of which are within 2 m s^{-1} of the observed ship and buoy wind speeds. For the remaining four comparisons, which are for rain flag 1 wind speeds, all but one fall within 3 m s^{-1}. In our sample, all of the SSM/I wind speeds less than 15 m s^{-1} fall within the ±2 m s^{-1} specification. For SSM/I wind speeds of at least 15 m s^{-1}, two out of three of the samples are within ±3 m s^{-1} of comparative ship and buoy observations. Overall, the SSM/I winds have a 1.28 m s^{-1} high bias with a standard deviation of 2.03 m s^{-1}.

For 23 overpasses of tropical cyclones, Holliday and Waters (1989) determined that the occurrences of SSM/I wind speeds less than 15 m s^{-1} lay within the ±2 m s^{-1} ground-truth specification for 70% of the samples. For SSM/I winds greater than or equal to 15 m s^{-1}, 82% were within ±3 m s^{-1} of comparative ship and buoy observations. Our samples here agree with the above assessment.

7. SSM/I center fixing estimations

The Florence case provided an excellent opportunity to test the utility of the higher-resolution (12.5 km) 85-GHz BT in estimating the center location of Florence. Velden et al. (1989) and Alliss et al. (1992) have both shown the value of using SSM/I data to determine tropical cyclone center locations. Because Florence was not a well-developed tropical cyclone, deep convective clouds were not organized near the center of circulation. This makes estimations of the center location using GOES IR and visible imagery somewhat difficult. SSM/I 85-GHz imagery, however, provided information on the low-level circulation characterized by a cyclonic twist of low clouds inward toward a center point.

Subjective SSM/I estimation of the center position has been conducted by determining the location of the low-level center as defined by the spiral-shaped signature in the 85-GHz channel near the storm center. Comparisons to NHC best-track data are made between 1) GOES IR estimates, made subjectively in non–real time without looping or aircraft reconnaissance data, and 2) SSM/I fixes. Because all of the SSM/I passes are either at 0000 or 1200 UTC, GOES visible imagery

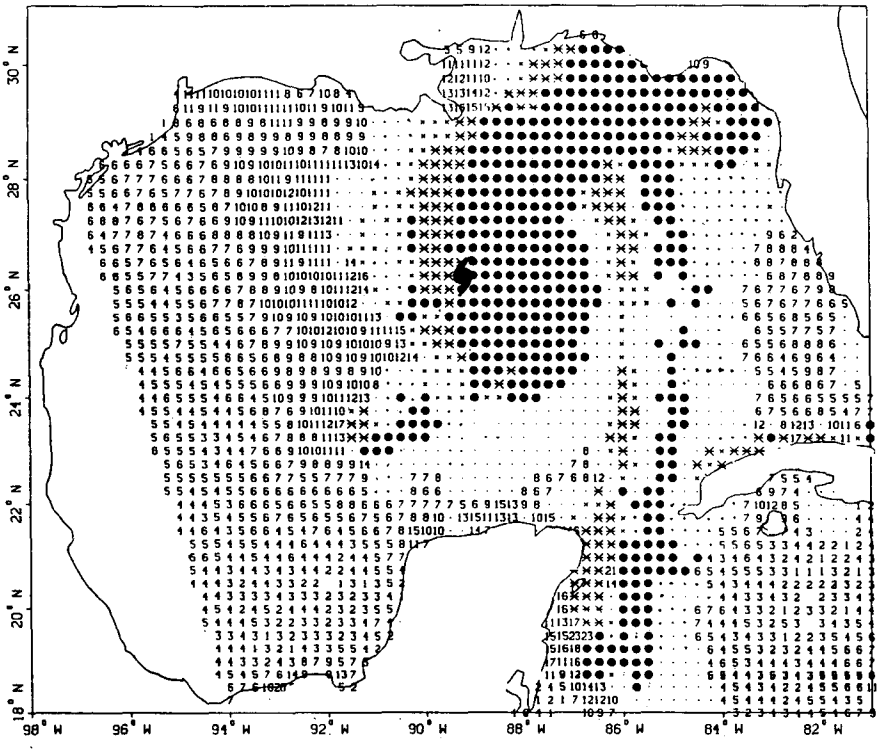

FIG. 9. Same as Fig. 8a except valid at 1200 UTC 9 September.

are not available for the comparison, only GOES IR imagery is used for the estimate. The results of the comparisons are presented Table 4. For the six passes, the average error, standard deviation σ, best case, and worst case are shown. The comparison shows that for the entire sample the average SSM/I estimate is much improved over the GOES IR estimate. In all cases, estimates made when using SSM/I are closer to NHC best-track data than when using GOES IR imagery. The mean errors of 65 km using the GOES IR imagery is improved to 19 km using the SSM/I 85-GHz imagery. It should be noted that there are only six fixes in this comparison and it is imperative that a larger sample of cases be examined to further assess in a statistically meaningful way the accuracy of using the 85-GHz imagery for center fixing. The 85-GHz imagery from the second and third SSM/I in orbit should also be used for comparison with GOES visible imagery for more recent cases.

8. Conclusions

SSM/I observations of rainfall have been used to analyze the precipitation patterns associated with Hurricane Florence of 1988. Based upon SSM/I precipitation estimates, the intensification of Florence is found to be accompanied by increases in the average rainfall, the relative contribution of heavier rainfall, and the total latent heat release. Unfortunately, the lag between the maximum TLHR and minimum pressure cannot be determined from these SSM/I observations due to Florence making landfall. SSM/I observations of Florence's precipitation field and its trend during intensification support those seen in the much larger and more intense Hurricane Hugo.

The surface wind field associated with Florence is analyzed using SSM/I marine surface wind speed data. SSM/I estimates that winds at 0000 UTC 9 September are generally lighter than an ODW-enhanced wind analysis valid for the approximately 950-mb level. On the other hand, SSM/I-derived wind speeds at 1200 UTC 9 September are slightly stronger than in situ observations over the Gulf of Mexico but the errors are well within specifications of algorithm validation. Due to the presence of heavy precipitation and cloud liquid water near the inner-core region, accurate maximum wind estimates from SSM/I are unavailable.

The ability of SSM/I 85-GHz imagery to provide much improved estimates of the location of Florence's center was clearly shown. Center position estimates using SSM/I imagery compared much better to the NHC best-track data than GOES IR imagery estimates.

TABLE 3. Latitude and longitude of available surface wind observations from Gulf of Mexico buoys and coastal stations at 1200 UTC 9 September 1988. SSM/I-estimated winds and rain flags (in parentheses) are also shown.

		Collocated wind observations (m s^{-1})	
Latitude (°N)	Longitude (°W)	Ship and buoy	SSM/I
26.0	93.5	8	6 (0)
26.0	86.0	15	17 (1)
28.8	89.2	16	19 (1)
24.5	82.0	8	9 (0)
27.2	82.5	4	5 (1)
29.3	94.8	3	4 (0)
26.0	89.7	20	24 (1)

TABLE 4. The average error, standard deviation (σ), best case, and worst case between NHC best-track positions and 1) GOES IR estimations, 2) SSM/I estimations. All values are in kilometers.

	GOES	SSM/I
Average error	65	19
Standard deviation	44	6
Best case	30	10
Worst case	162	26

Acknowledgments. We thank Mr. Jainn-Jong Shi of North Carolina State University (NCSU) for providing the enhanced dropsonde wind analysis and Mr. Kevin Schrab, also of NCSU, for assistance in the statistical analysis. The research was supported by SPAWAR (6370 X-1596-0932), NRL (basic research program), and ONR (N00014 92 AF002).

REFERENCES

Alliss, R. A., S. W. Chang, and S. Raman, 1992: Special Sensor Microwave/Imager (SSM/I) observations of Hurricane Hugo (1989). *Mon. Wea. Rev.*, **120,** 2723–2737.

Goodberlet, M. A., C. T. Swift, and J. C. Wilkerson, 1989: Remote sensing of ocean surface winds with the Special Sensor Microwave/Imager. *J. Geophys. Res.*, **94,** 547–555.

Holliday, C. R., and K. R. Waters, 1989: SSM/I observations of tropical cyclone gale force vicinity winds. *Proc., Fourth Conf. on Satellite Meteor. and Oceanography,* Amer. Meteor. Soc., San Diego, 267–270.

Hollinger, J. P., 1989: DMSP Special Sensor Microwave/Imager Calibration Validation, Final Report Vol. II. [Available from Simon Chang, Naval Research Laboratory, Washington, D.C. 20375.]

Lawrence, M. B., and J. M. Gross, 1989: Annual summaries: Atlantic hurricane season of 1988. *Mon. Wea. Rev.*, **117,** 2248–2259.

Olson, W. S., 1989: Physical retrieval of rainfall rates over the ocean by multispectral microwave radiometry—Application to tropical cyclones. *J. Geophys. Res.*, **94,** 2267–2280.

Rodgers, E. B., and R. F. Adler, 1981: Tropical cyclone rainfall characteristics as determined from a satellite passive microwave radiometer. *Mon. Wea. Rev.*, **109,** 506–521.

——, S. Chang, J. Stout, J. Steranka, and J. J. Shi, 1991: Satellite observations of variations in tropical cyclone convection caused by upper-tropospheric troughs. *J. Appl. Meteor.*, **30,** 1163–1184.

Shi, J-J., S. Chang, K. Sashegyi, and S. Raman, 1991: Enhancement of objective analysis of Hurricane Florence (1988) with dropsonde data. *Proc. 19th Conf. of Hurricanes and Tropical Meteorology,* Amer. Meteor. Soc., Miami, FL, 335–337.

Velden, C. S., W. S. Olson, and B. A. Roth, 1989: Tropical cyclone center-fixing using SSM/I data. Proc., Fourth Conf. on Satellite Meteor. and Oceanography, San Diego, 36–39.